The NMR structure of the 47-kDa dimeric enzyme 3,4-dihydroxy-2-butanone-4-phosphate synthase and ligand binding studies reveal the location of the active site

Mark J. S. Kelly*†‡, Linda J. Ball*, Cornelia Krieger§, Yihua Yu†¶, Markus Fischer§, Susanne Schiffmann§, Peter Schmieder*, Ronald Kühne*, Wolfgang Bermel‖, Adelbert Bacher§, Gerald Richter‡§, and Hartmut Oschkinat*‡

*Research Institute for Molecular Pharmacology, Robert-Rössle-Strasse 10, D-13125 Berlin, Germany; §Lehrstuhl für Organische Chemie und Biochemie, Technical University Munich, D-85747 Garching, Germany; †European Molecular Biology Laboratory, Meyerhof-Strasse 1, D-69117 Heidelberg, Germany; and ‖Bruker Analytische Messtechnik GmbH, Silberstreifen, D-76287 Rheinstetten, Germany

Edited by Robert Huber, Max Planck Institute for Biochemistry, Martinsried, Germany, and approved September 10, 2001 (received for review June 26, 2001)

Recent developments in NMR have extended the size range of proteins amenable to structural and functional characterization to include many larger proteins involved in important cellular processes. By applying a combination of residue-specific isotope labeling and protein deuteration strategies tailored to yield specific information, we were able to determine the solution structure and study structure–activity relationships of 3,4-dihydroxy-2-butanone-4-phosphate synthase, a 47-kDa enzyme from the *Escherichia coli* riboflavin biosynthesis pathway and an attractive target for novel antibiotics. Our investigations of the enzyme's ligand binding by NMR and site-directed mutagenesis yields a conclusive picture of the location and identity of residues directly involved in substrate binding and catalysis. Our studies illustrate the power of state-of-the-art NMR techniques for the structural characterization and investigation of ligand binding in protein complexes approaching the 50-kDa range in solution.

enzymology | drug design | structure–activity relationships | antibiotic | isotope labeling

Novel drugs directed against microbial targets are required urgently to keep pace with the emergence of antibiotic resistance. Attractive intervention strategies include those that target specific biosynthetic pathways present only in pathogens. The riboflavin biosynthetic pathway, common to a number of plants and microorganisms but entirely absent in animals who acquire this vitamin from their diet, constitutes an ideal target for designed inhibitory drugs.

The complex reaction mechanism of 3,4-dihydroxy-2-butanone-4-phosphate synthase (DHBPS, EC 5.4.99; refs. 1 and 2), which is one of the enzymes involved in microbial riboflavin biosynthesis, provides promising opportunities for the design of mechanism-based inhibitors as lead compounds for a new generation of antibiotic or antimycotic drugs. DHBPS is a homodimer in solution (3), is comprised of two identical 23-kDa subunits that show a single set of resonances for backbone nuclei in NMR spectra, and requires Mg^{2+} for catalytic activity (4, 5). Although the three-dimensional structure of DHBPS was determined recently by x-ray crystallography (6), the identity of the active site remains to be identified conclusively.

The wider application of NMR to investigate structure–activity relationships in larger proteins and to isolate ligands from chemical libraries, however, has been hindered severely by size limitations. By using protein deuteration strategies combined with state-of-the-art NMR methods, we achieved resonance assignment and determined the solution structure of DHBPS (47 kDa) from *Escherichia coli*. We subsequently used NMR chemical shift mapping to identify the active site and used it to guide site-directed mutagenesis experiments to highlight the residues essential for catalysis. These key new functional data are paramount to an understanding of the complex catalytic mechanism of DHBPS and the design of potent new inhibitors.

Methods

Preparation of Isotope-Labeled Samples of DHBPS and NMR Spectroscopy. Isotope-labeled DHBPS proteins were expressed in *E. coli* and purified as described previously (3, 7–9). NMR spectra were acquired at 313 K by using Bruker DRX600 and DMX750 spectrometers. Backbone and side chain assignment experiments for ^{2}H-, ^{13}C-, and ^{15}N-labeled proteins (7, 10) and nuclear Overhauser effect (NOE) experiments (τ_m = 70–100 ms) were performed as described previously (7, 11). A 200-ms three-dimensional $^{15}N/^{15}N$-heteronuclear single quantum correlation (HSQC)-NOE spectroscopy (NOESY)-HSQC experiment on a [U-^{2}H]- and [U-^{15}N]-DHBPS protein (12) and a 200-ms three-dimensional CT-^{13}C edited NOESY (13) recorded on a sample with methyl protonation of Val, Leu, and Ile (C_δ) methyl groups [NOEs from these were not quantified (14) and values of ≤6.8 and ≤6.0 Å were used, respectively]. The data processing and assignment programs used were XWIN-NMR 1.3 (Bruker Analytik GmbH, Rheinstetten, Germany), AZARA (W. Boucher, unpublished data), and ANSIG 3.3 (15).

Structure Calculations. Structures were calculated (Table 1) with the program CNS 1.0 (16). Distance restraints were categorized as strong (≤2.5 Å), medium (≤3.5 Å), weak (≤4.5 Å), and very weak (≤6.0 Å). Dihedral angle restraints were from backbone chemical shifts after correction for the deuteration (14, 17–19). Sixty-nine hydrogen-bond restraints were identified from a two-dimensional ^{15}N HSQC spectrum 96 h after exchange from H_2O to D_2O.

This paper was submitted directly (Track II) to the PNAS office.

Abbreviations: DHBPS, 3,4-dihydroxy-2-butanone-4-phosphate synthase; NOE, nuclear Overhauser effect; HSQC, heteronuclear single quantum correlation; NOESY, NOE spectroscopy.

Data deposition: The atomic coordinates and structure factors have been deposited in the Protein Data Bank, www.rcsb.org (PDB ID code 1IEZ).

‡To whom reprint requests may be addressed. E-mail: oschkinat@fmp-berlin.de or kelly@fmp-berlin.de.

¶Present address: Institute for Organic Chemistry, Chinese Academy of Sciences, 354 Fenglin Lu, Shanghai 200032 China.

The publication costs of this article were defrayed in part by page charge payment. This article must therefore be hereby marked "*advertisement*" in accordance with 18 U.S.C. §1734 solely to indicate this fact.

BIOPHYSICS

Table 1. Restraints and structural statistics for the final DHBPS ensemble

Restraints		
Total experimental restraints	1109	
Total interresidue NOE restraints	674	
Sequential ($\|i - j\| = 1$)	295	
Medium range ($1 < \|i - j\| \leq 4$)	139	
Long range ($\|i - j\| > 4$)	240	
H-bond restraints	67	
Dihedral angle restraints	297	
NOE violations > 0.5 Å	0	
Dihedral angles $> 20°$	0	
ϕ/ψ space: residues*		
Most favored regions, %	68.7	
Additionally allowed regions, %	20.3	
Generously allowed regions, %	7.1	
Residues in disallowed regions, %	3.9	
Energies		
Final energies, kcal/mol	$(SA)_{ensemble}$†	$\langle SA \rangle_{s.c.m.}$‡
E_{bonds}	25.69 ± 5.17	28.57
E_{angles}	181.74 ± 46.8	202.58
$E_{impropers}$	33.93 ± 12.4	39.67
E_{vdW}	187.17 ± 39.49	218.24
E_{NOE}	58.35 ± 12.06	59.78
rmsds§		
Deviation from ideal values		
Bonds	0.0028 ± 0.0003	0.003
Angles	0.4487 ± 0.0565	0.475
Impropers	0.3665 ± 0.0655	0.399
Backbone¶	2.28 ± 0.51	1.5

*Calculated with PROCHECK-NMR (32).

†$(SA)_{ensemble}$ represents the average r.m.s. deviations for the ensemble of 8 structures.

‡$\langle SA \rangle_{s.c.m.}$ are the statistics for the structure closest to the mean.

§Evaluated by CNS (16).

¶Mean global backbone (2.28 ± 0.51) and average rmsd to mean structure (1.5, average) calculated with the program MOLMOL (31). In the rmsd calculations the following residues were used: Thr-4–Val-31, Met-43–Val-84, Gly-94–Thr-176, Ala-185–Arg-214.

NMR Chemical Shift Mapping Experiments. The binding of Mg^{2+} cofactor (20 mM $MgCl_2$), substrate (25 mM D-ribulose-5-phosphate, Sigma), and product were investigated by using two-dimensional ^{15}N HSQC spectra. The combined chemical shift perturbations ($\Delta\delta_{TOTAL}$) of all ^{1}H and ^{15}N resonances were weighted according to ref. 20 and grouped into two classes (see Fig. 3 legend).

Site-Directed Mutagenesis. Mutant DHBPS proteins from *Methanococcus jannaschii* were expressed in *E. coli*, and enzyme activities were assayed as described previously (21).

Results and Discussion

Rapid ^{13}C relaxation and the sheer number of nuclei present in DHBPS (47 kDa) lead to highly complex, overlapped NMR spectra containing signals with broad line widths. Furthermore, strong ^{1}H–^{1}H dipolar interactions in larger proteins can lead to a reduction in the accuracy of NOE-based distance restraints (22, 23) and preclude the observation of long range correlations (24). Overcoming these problems by protein deuteration was crucial to facilitate structure determination; we therefore applied multidimensional heteronuclear NMR methods together with a series of strategically designed samples [random fractional deuteration (75% ^{2}H) combined with $^{13}C/^{15}N$ labeling, residue-specific protonation in an ^{15}N-labeled deuterated background, and a sample with methyl protonation of Val, Leu and Ile (C_δ) in a deuterated background; refs. 7–9] tailored to improve and simplify NMR spectra. The application of random fractional deuteration to improve ^{13}C relaxation was essential for the successful application of triple-resonance experiments (INEPT transfer; refs. 7, 10, 11, and 17) that correlated 196 amide proton and nitrogen pairs with the sequential and previous residue's C_α, C_β, and C′ resonances. Sequential assignment was possible for 169 of them together with the assignment of many of their side chain signals (30% of ^{1}H and 60% of ^{13}C nuclei) by using a compromise level of 75% random fractional deuteration and $^{13}C/^{15}N$ labeling (7). The identities of the remaining 27 unassigned correlations were easily identified by inspecting spectra from two samples in which either Phe, Tyr, Thr, Ile, and Val (8) or Phe and Pro were incorporated as protonated (^{14}N) amino acids in a fully deuterated and ^{15}N-labeled background (8). By using this approach it was possible to assign 196 backbone resonances and more than 70% of their side chain signals (^{1}H and ^{13}C nuclei) including all Val, Leu, Ile, Phe, and Tyr residues (with the exception of Tyr-91) and the majority of C_α, C_β, H_α, and H_β signals for the eight prolines. The majority of unassigned residues were located in two regions of the sequence (32–42 and 83–94). Repeating some of the triple resonance experiments with transverse relaxation-optimized spectroscopy-based sequences (25) did not provide more correlations, probably because of the line widths of the missing signals.

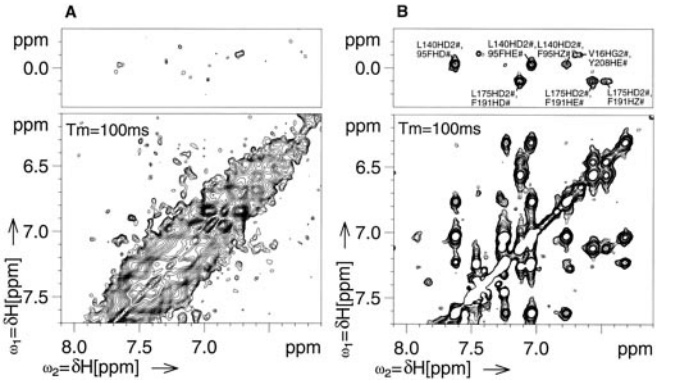

Fig. 1. Two-dimensional 100-ms NOESY spectra of DHBPS. The regions show the aromatic protons (*Lower*) and long range correlations from aromatics to methyl protons (*Upper*). Spectra from a sample with 75% random fractional deuteration, $^{13}C/^{15}N$ labeling (*A*) and a sample with protonated Phe, Tyr, Thr, Ile, and Val in a fully protonated and ^{15}N-labeled background (*B*) are shown.

NOE distance restraints were collected from all three types of deuterated samples. The sample with 75% random fractional deuteration (and $^{13}C/^{15}N$ labeling) yielded many medium distance (<4.0 Å) constraints of the type H_α–HN and HN–HN with good accuracy as well as long range ($>i, i + 3$) interactions between carbon-bound protons. On the contrary, rapid relaxation of aromatic protons by their directly coupled ^{13}C spins (26) and proton dilution (deuteration) prevented the observation of key NOEs between methyl groups and aromatic ring protons using this sample (Fig. 1*A*). Such correlations were easily obtained by using two samples without ^{13}C labeling, where either Phe, Tyr, Thr, Ile and Val (8) or Phe and Pro were incorporated into a fully deuterated background (Fig. 1*B*). Because of their simpler spectra and greater sensitivity, the samples with residue-specific labeling contributed many more important restraints. Resonance degeneracy also complicated the assignment of important NOEs between the many methyl

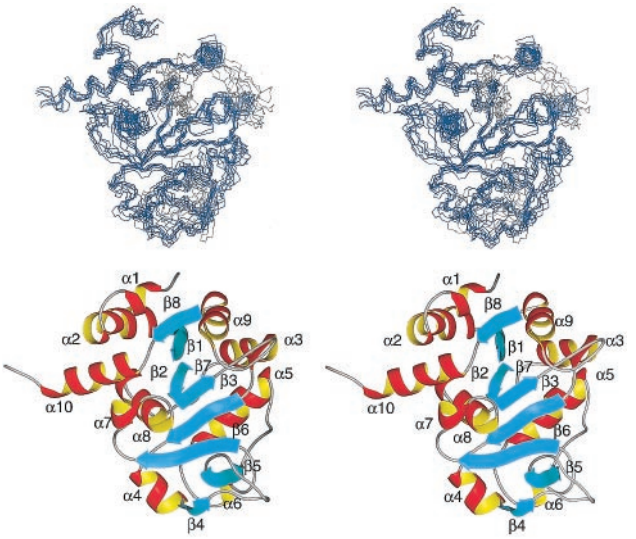

Fig. 2. (*A*) Ensemble of the eight lowest energy structures of the DHBPS monomer. Three loops (31–43, 84–94, and 176–185) and the N and C termini for which no long range NOE correlations were observed are marked in black. (*B*) Ribbon (MOLMOL; ref. 31) diagram of the DHBPS monomer.

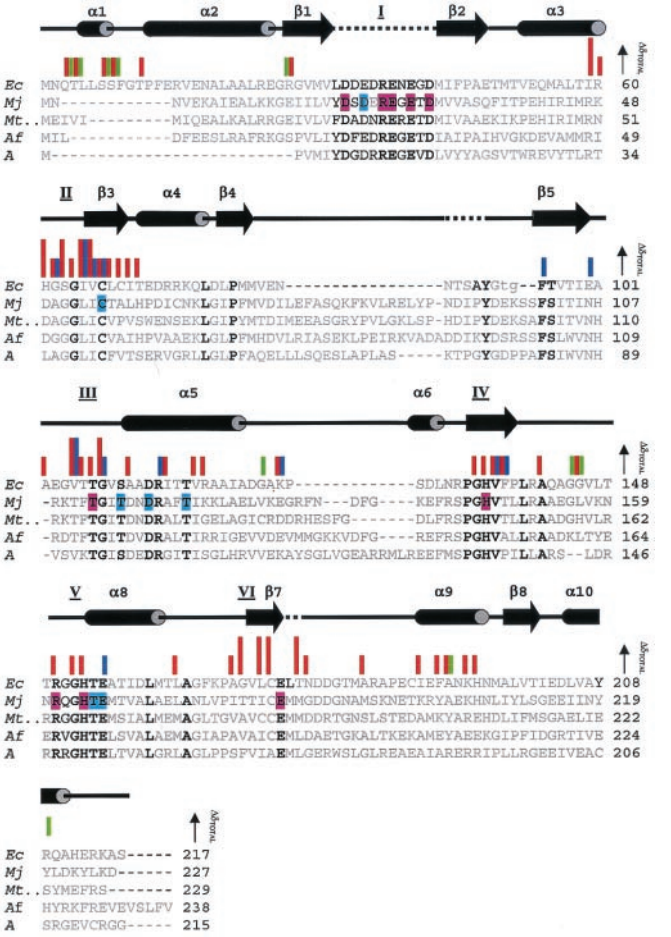

Fig. 3. Sequence alignments of four divergent members of the DHBPS family. Residues strictly conserved in 20 sequences are shown in bold (*Ec*, *E. coli*; Mj, *M. jannaschii*; Mt, *Methanobacterium thermoautotrophicum*; Af, *Archaeoglobus fulgidus*; A, *Aeropyrum*). The secondary structure of the *E. coli* enzyme is shown above the sequence. Results from NMR chemical shift mapping experiments investigating the binding of ligands is indicated by bars (red, blue, and green) above the sequence. The combined chemical shift perturbations ($\Delta\delta_{TOTAL}$) of all ^{1}H and ^{15}N resonances were weighted according to $\Delta\delta_{TOTAL} = \Delta\delta\,[^1H] + 0.2\,\Delta\delta\,[^{15}N]$ (20) and grouped into two classes (moderate, short bars $\Delta\delta_{TOTAL} = 0.06–0.12$ ppm and strong, tall bars $\Delta\delta_{TOTAL} > 0.12$ ppm). Red bars show the location and magnitude of chemical shift changes on the addition of the substrate, ribulose-5-phosphate, in the presence of Mg^{2+} ions. Blue bars indicate signals affected after the addition of substrate in the absence of Mg^{2+}. Green bars indicate perturbations after the addition of Mg^{2+}. The backbone nuclei of the residues that were not assigned in NMR spectra are marked with a dashed line in the secondary structure. Amino acids that, when substituted in the *M. jannaschii* sequence by site-directed mutagenesis, led to a loss of catalytic activity are highlighted in red, and those leading to significantly reduced activity are highlighted in cyan.

groups. Three-dimensional NOESY experiments with CT-^{13}C-evolution periods (13) using a sample with site-specific protonation of the Val, Leu, and Ile (C_δ) methyl groups in a fully deuterated background (9) provided a large number of unambiguous long range NOEs. Together with data from the samples with residue-specific labeling, these restraints defined the fold already in the early stages of structure determination.

A single set of signals was identified for all backbone and side chain nuclei consistent with a dimeric protein (3) with C_2 symmetry. Our attempts to mix monomers with different isotopic labeling patterns yielded an enzyme with low specific activity. Without recourse to this approach, intermonomer NOEs can be identified only where they arise from protons that are too far apart in the monomer structure to give rise to intramonomer NOEs (>6 Å; refs. 27). Such NOEs, however, were not found. The observation that some resonances (83, 88, 90, 91, 174, and 175) corresponding to amino acids close to the crystallographic dimer interface (6) were absent from NMR spectra could be an indication of movement of the two monomers relative to each other, perhaps leading to attenuation of intermonomer NOEs.

The solution structure of DHBPS (Fig. 2*A*) was calculated on the basis of 674 interresidue NOE distance constraints (Table 1). The number of unambiguous NOEs distance restraints assigned was limited to this number because of (*i*) the large signal degeneracy caused by the large α-helical content and the relatively low number of aromatic residues, (*ii*) the absence of NOE contacts involving residues in two regions of the protein (conserved stretch of acidic residues 32–42 and 83–95), (*iii*) resonances for some residues only being present in spectra from samples without ^{13}C labeling, (*iv*) the use of residue-specific labeling for only two subsets of amino acids, and (*v*) the removal of certain protons by deuteration. The protein possesses a unique α-β fold [DALI (28) Z scores < 0.7 and CATH (29) scores >18] with a complex topology comprised of a central mixed eight-stranded β-sheet onto which 10 α-helices pack (Fig. 2*B*). From visual inspection, the solution structure determined by NMR is very similar to that very recently reported by Liao *et al.* (ref. 6; the atomic coordinates of the x-ray structure were not available during our study). No signals were found in our NMR spectra for a loop formed by a stretch of highly conserved acidic residues joining strands β1 and β2 (DDEDRENEGD, residues 33–42). Signal broadening of flanking residues suggests local motions with intermediate conformational exchange characteristics. Interestingly, Liao *et al.* also reported no electron density corresponding to the region Asp-34–Asn-39 (6).

To identify the location of the active site, which was not forthcoming from the x-ray structure determined in the absence of ligand (6), we used NMR to map the specific locations of the binding sites for the substrate, product, and Mg^{2+} cofactor. We took advantage of the absolute requirement of the Mg^{2+} cofactor for catalysis to observe enzyme–ligand interactions under

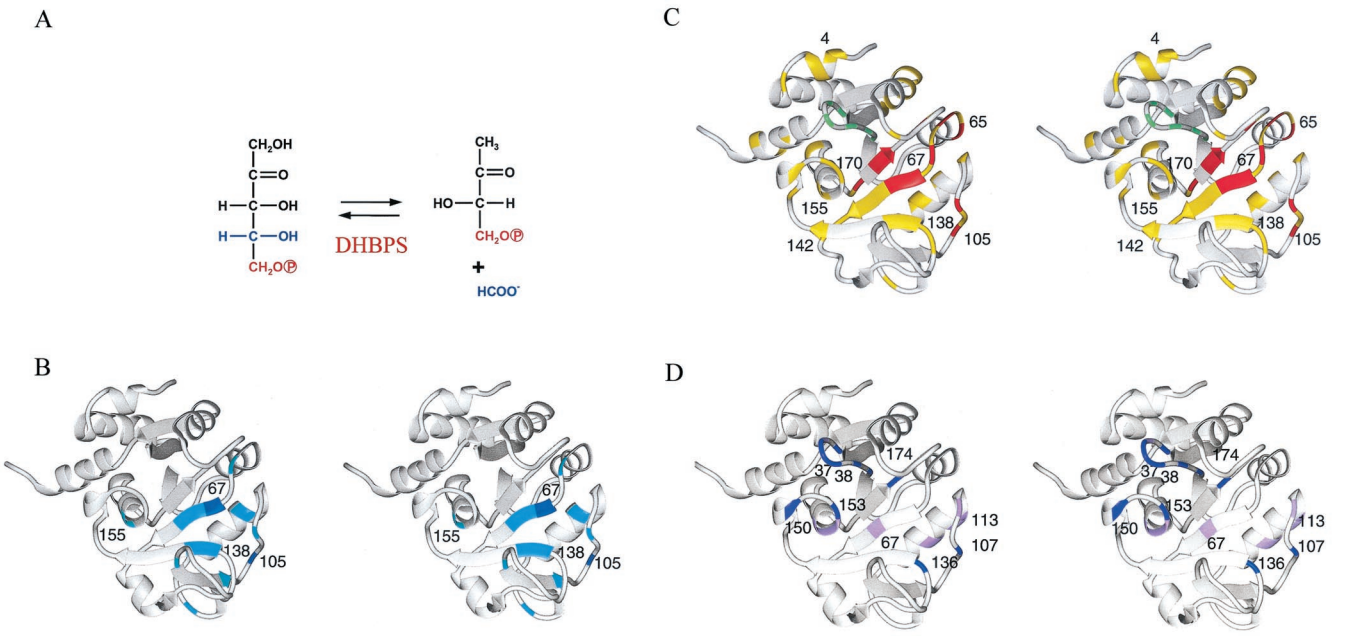

Fig. 4. Data from chemical shift mapping experiments investigating ligand binding and mutations with reduced activity mapped onto the three-dimensional structure depicted as a ribbon diagram (MOLMOL; ref. 31). Residues with strong ($\Delta\delta_{TOTAL} > 0.12$ ppm) or moderate (moderate $\Delta\delta_{TOTAL} = 0.06–0.12$ ppm) chemical shift perturbations after addition of ligands and complete or significant loss in activity after mutation are marked in dark and light colors, respectively. The conserved acidic loop joining strands β1 and β2 is indicated by green stripes. (*A*) The reaction catalyzed by DHBPS. (*B*) Chemical shift mapping of substrate binding to the enzyme in the absence of Mg^{2+} (nonturnover conditions). Strong and moderate shifts (see Fig. 3) are shown in blue and cyan, respectively. (*C*) Chemical shift mapping of product binding to the enzyme and catalysis in the presence of Mg^{2+} (turnover conditions). Strong and moderate shifts (see Fig. 3) are shown in red and yellow, respectively. (D) Results of site-directed mutagenesis experiments. Residues that, when substituted in the *Methanococcus* sequence, led to a loss of catalytic activity and those with a significant reduction in activity are shown in magenta and pink, respectively (see Table 2).

both turnover (in the presence of Mg^{2+}) and substrate binding (in the absence of divalent cations, 20 mM EDTA) conditions, which cannot normally be separated experimentally because of the conversion of substrate into product (Fig. 4*A*). In our case, no conversion of substrate into product takes place in the absence of divalent cations. Three separate experiments were conducted: (*i*) location of the substrate binding site under conditions in which catalysis was prevented by removal of divalent cations from the enzyme (20 mM EDTA; Fig. 4*B*), (*ii*) identification of residues involved in catalysis and product binding (Fig. 4*C*), and (*iii*) identification of Mg^{2+} binding sites by comparison of NMR spectra in the presence and absence of Mg^{2+}. The combined chemical shift perturbations on ligand binding ($\Delta\delta_{TOTAL}$) of all ^1H and ^{15}N resonances were weighted according to $\Delta\delta_{TOTAL} = \Delta\delta[^1H] + 0.2\,\Delta\delta[^{15}N]$ (20) and grouped into two classes (Fig. 2; moderate, short bars $\Delta\delta_{TOTAL} = 0.06–0.12$ ppm and strong, tall bars $\Delta\delta_{TOTAL} > 0.12$ ppm).

Changes in the positions of signals in the NMR spectra revealed the substrate binding site in the absence of cofactor (Fig. 3 and 4*B*), with a stretch of amino acids flanking the conserved Cys-67, exhibiting the greatest density of shifts. Under turnover conditions (addition of substrate 25 mM D-ribulose-5-phosphate in the presence of 20 mM $MgCl_2$), distinct chemical shift changes of larger magnitude were observed (Figs. 3 and 4*C*) for the same residues found to contact substrate (marked in red in Fig. 4*C*). In our case, turnover conditions are dominated by the presence of products, because the reaction liberates two molecules (formic acid and product) from one of substrate (Fig. 4*A*), and therefore the reverse reaction is disfavored for entropic reasons. Our data clearly show that both substrate and products bind to residues in the same region of the three-dimensional structure (Fig. 4 *B* and *C*), and although Mg^{2+} is essential for activity, its presence is not vital for substrate binding. In addition, perturbations of signals from two arginine Hε protons were observed, which could belong to two of the three conserved arginines (Arg-37, Arg-114, and Arg-150). Under turnover conditions, changes in chemical shifts in many cases were accompanied by significant broadening of signals in the spectra (residues 61–71, 107–109, 136–138, 150–155, 170, 172, 173, 176, 177, and 183). This effect is strongly indicative of ligand binding. After the addition of the Mg^{2+} cofactor in the absence of substrate, chemical shift perturbations could be monitored for residues at the N terminus of the protein (Gln-3, Thr-4, and Leu-5; Fig. 3). These residues also show chemical shift changes under turnover conditions because of the presence of Mg^{2+} (Fig. 4*C*). However, this binding site is unlikely to be catalytically relevant, because it is not present in all members of the DHBPS family. The most likely explanation for the lack of chemical shift changes elsewhere in the protein after Mg^{2+} addition is that the catalytically important Mg^{2+} binding site is located in the conserved stretch of acidic residues (33–42) and possibly Glu-174, for which no signals could be seen in the NMR spectra (see below).

Site-directed mutagenesis allowed us to pinpoint residues in regions showing chemical shift perturbations that are essential for enzymatic activity of DHBPS. Criteria in choosing the sites for mutations were (*i*) NMR-guided (conserved residues with large chemical shift changes), (*ii*) structure-guided (surface-exposed residues), and (*iii*) to investigate whether the stretch of highly conserved acidic residues (for which neither NMR nor x-ray data are available) is involved in catalysis. The mutagenesis studies were carried out by using DHBPS from *M. jannaschii*, which has 29% amino acid identity with the *E. coli* enzyme (Fig. 3). The results of these studies are summarized in Table 2. The residues, which after mutation abolished

Table 2. Activities of *Methanococcus* DHBPS mutants
All numbering based on *E. coli* DHBPS (see Fig. 3). n.d., activities were below the detection limit of the assay.

		% of wild-type activity
	Wild type	100
Region I	D33S	n.d.
	D35S	16
	R37E	n.d.
	E38S	n.d.
	E40S	n.d.
	D42S	n.d.
Region II	C67S	19
Region III	T107S	n.d.
	T110A	16
	D113S	12
	T117A	26
Region IV	H136S	n.d.
Region V	R150S	n.d.
	H153S	n.d.
	T154A	32
	E155S	17
Region V	E174S	n.d.

enzyme activity (i.e., marked in dark purple in Fig. 4*D*) or resulted in significant reduction in activity (<30% of wild-type activity, marked in pink, Fig. 4*D*), confirmed the data obtained by NMR analysis of the *E. coli* enzyme. Notably, single mutations of residues (D33S, R37E, E38S, E40S, and D42S) in the conserved acidic region not visible in either the NMR or the x-ray data (6) completely abolished activity. Consistent with these data the nearby conserved Glu-174 (for which we have no NMR assignments; however, flanking residues show significant chemical shift changes) was found to be essential.

The short loop of catalytically important conserved acidic residues (32–42) connects two antiparallel β-strands (β1 and β2), which are well defined by the NMR constraints, restricting its position (dashed line in Fig. 4*C*). This suggests that the side chains of these residues probably ligating the Mg^{2+} cofactor, could come close to the other active site residues to form a cluster (Fig. 4*C*). In summary, our results suggest that the active site consists of residues involved in acid/base catalysis and substrate recognition (Arg-37, Cys-67, Arg-114, His-136, Arg-150, and His-153), hydrogen-bonding interactions with the substrate (Thr-107), and ligation of Mg^{2+} cofactor (Asp-33, Glu-38, Glu-40, Asp-42, and Glu-174). Although it is possible that some mutations could lead to a loss in activity through structural changes, our proposals are supported by the close agreement of the NMR and mutational data.

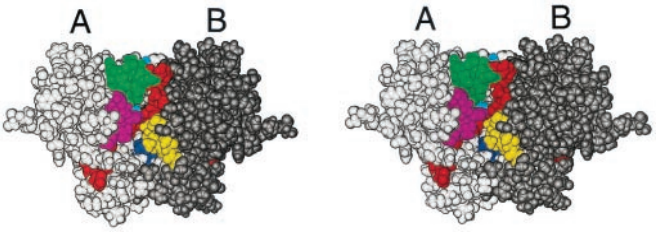

Fig. 5. Space-filled representation (MOLMOL; ref. 31) of the dimer model built using the monomeric NMR structure. The model satisfies the intermolecular contacts reported by Liao *et al.* (6). The active site shown on the front of the dimer is formed by the regions showing large chemical shift changes on ligand binding: I, 32–42, green; II, 59–71, red; V, 150–155, magenta; VI, 170–176, cyan, from monomer A; III, 105–113, yellow; IV, 135–138, blue, from monomer B.

The dimeric nature of the enzyme has implications for substrate binding and catalysis. Notably the two catalytic residues Thr-107 and His-136 are separated spatially from the cluster of essential acidic and basic amino acids and Cys-67 in the monomer. To help visualize the locations of residues important for catalysis, we built a dimer model by using our monomer structure, which satisfies the intermolecular contacts described by Liao *et al.* (ref. 6; hydrophobic interactions: Ile-65, Met-83, Val-84, Phe-95, Val-97, and Phe-138; H-bonding interactions: Thr-107–Glu-40, Arg-114–Ser-63, and Gly-64, and His-136–Glu-174; the coordinates of the x-ray structure were not available at this time). In our model (Fig. 5) the two groups of spatially separated residues (Asp-33, Arg-37, Glu-38, Glu-40, Asp-42, Cys-67, Arg-150, His-153, and Thr-107 and His-136) are brought together to form the active site. The acidic and basic residues in the cluster are on one side of the putative binding pocket facing Cys-67 and His-136. This knowledge will facilitate the understanding of the complex catalytic mechanism, the design of transition-state inhibitors, and the potential development of a new generation of antibiotics. Our studies of this 47-kDa enzyme provide a convincing demonstration of how recent advances in NMR methods (30) have opened the way to structure–activity relationships of larger complexes and enzymes in solution as well as the study of their ligand binding properties and protein–protein interactions.

BIOPHYSICS

We thank Ernest Laue, Daniel Nietlispach, Peter Domaille, Lewis Kay, Geoffrey Mueller, Ronald Venters, and Tanja Kortemme for many stimulating and helpful discussions. Jürgen Zimmermann is thanked for critical reading of the manuscript. Goran Karlsson is acknowledged for initial experiments. M.J.S.K. was supported by the European Molecular Biology Organization and The Wellcome Trust. L.J.B. thanks the European Molecular Biology Organization for support. Deutsche Forschungsgemeinschaft and Bundesministerium für Bildung, Wissenschaft, Forschung und Technologie are gratefully acknowledged for financial support.

1. Bacher, A., Eberhardt, S., Fischer, M., Kis, K. & Richter, G. (2000) *Annu. Rev. Nutr.* **20,** 153–167.
2. Götze, E., Kis, K., Eisenreich, W., Yamauchi, N., Kakinuma, K. & Bacher, A. (1998) *J. Org. Chem.* **63,** 6456–6457.
3. Richter, G., Kelly, M., Krieger, C., Yu, Y., Bermel, W., Karlsson, G., Bacher, A. & Oschkinat, H. (1999) *Eur. J. Biochem.* **261,** 57–65.
4. Volk, R. & Bacher, A. (1988) *J. Am. Chem. Soc.* **110,** 3651–3653.
5. Volk, R. & Bacher, A. (1990) *J. Biol. Chem.* **265,** 19479–19485.
6. Liao, D. I., Calabrese, J., Wawrzak, Z., Viitanen, P. V. & Jordan, D. B. (2001) *Structure (London)* **9,** 11–18.
7. Nietlispach, D., Clowes, R. T., Broadhurst, W., Ito, Y., Keeler, J., Kelly, M., Ahurst, J., Oschkinat, H., Domaille, P. J. & Laue, E. D. (1996) *J. Am. Chem. Soc.* **118,** 407–415.
8. Kelly, M. J., Krieger, C., Ball, L. J., Yu, Y., Richter, G., Schmieder, P., Bacher, A. & Oschkinat, H. (1999) *J. Biomol. NMR* **14,** 79–83.
9. Goto, N. K., Gardner, K. H., Mueller, G. A., Willis, R. C. & Kay, L. E. (1999) *J. Biomol. NMR* **13,** 369–374.
10. Yamazaki, T., Lee, W., Arrowsmith, C. H., Muhandirum, D. R. & Kay, L. E. (1994) *J. Am. Chem. Soc.* **116,** 11655–11666.
11. Kay, L. E. (1997) *Biochem. Cell Biol.* **75,** 1–15.
12. Mal, T. K., Matthews, S. J., Kovacs, H., Campbell, I. D. & Boyd, J. (1998) *J. Biomol. NMR* **12,** 259–276.
13. Zwahlen, C., Gardner, K. H., Sarma, P. S., Hortita, D. A., Byrd, R. A. & Kay, L. E. (1998) *J. Am. Chem. Soc.* **120,** 7617–7625.
14. Mueller, G. A., Choy, W. Y., Yang, D., Forman-Kay, J. D., Venters, R. A. & Kay, L. E. (2000) *J. Mol. Biol.* **300,** 197–212.
15. Kraulis, P. J., Domaille, P. J., Campbell-Burk, S. L., Van Aken, T. & Laue, E. D. (1994) *Biochemistry* **33,** 3515–3531.
16. Brunger, A. T., Adams, P. D., Clore, G. M., DeLano, W. L., Gros, P., Grosse-Kunstleve, R. W., Jiang, J. S., Kuszewski, J., Nilges, M., Pannu, N. S., *et al.* (1998) *Acta Crystallogr. D* **54,** 905–921.
17. Venters, R. A., Farmer, B. T., II, Fierke, C. A. & Spicer, L. D. (1996) *J. Mol. Biol.* **264,** 1101–1116.

18. Cornilescu, G., Delaglio, F. & Bax, A. (1999) *J. Biomol. NMR* **13,** 289–302.
19. Wishart, D. S. & Sykes, B. D. (1994) *J. Biomol. NMR* **4,** 171–180.
20. Hajduk, P. J., Dinges, J., Miknis, G. F., Merlock, M., Middleton, T., Kempf, D. J., Egan, D. A., Walter, K. A., Robins, T. S., Shuker, S. B., *et al.* (1997) *J. Med. Chem*. **40,** 3144–3150.
21. Richter, G., Volk, R., Krieger, C., Lahm, H.-W., Röthlisberger, U. & Bacher, A. (1992) *J. Bacteriol.* **174,** 4050–4056.
22. Wagner, G. (1993) *J. Biomol. NMR* **3,** 375–385.
23. Madrid, M., Mace, J. E. & Jardetzky, O. (1989) *J. Magn. Reson.* **83,** 267–278.
24. Pachter, R., Arrowsmith, C. H. & Jardetzky, O. (1992) *J. Biomol. NMR* **2,** 183–194.
25. Pervushin, K. (2000) *Q. Rev. Biophys.* **33,** 161–197.
26. Vuister, G. W., Kim, S.-J. & Bax, A. (1994) *J. Am. Chem. Soc.* **116,** 9206–9210.
27. O'Donoghue, S. I. & Nilges, M. (1999) in *Biological Magnetic Resonance*, eds. Krishna, N. R. & Berliner, L. J. (Kluwer, New York), Vol. 17, pp. 131–161.
28. Holm, L. & Sander, C. (1993) *J. Mol. Biol.* **233,** 123–138.
29. Gilbert, D., Westhead, D., Nagano, N. & Thornton, J. (1999) *Bioinformatics* **15,** 317–326.
30. Gardner, K. H. & Kay, L. E. (1998) *Annu. Rev. Biophys. Biomol. Struct.* **27,** 357–406.
31. Koradi, R., Billeter, M. & Wuthrich, K. (1996) *J. Mol. Graphics* **14,** 51–55.
32. Laskowski, R. A., Rullmann, J. A., MacArthur, M. W., Kaptein, R. & Thornton, J. M. (1996) *J. Biomol. NMR* **8,** 477–486.